Interpretation of the neutron double-differential cross sections in the interactions of $p+$Al, Fe, and Zr at 1.2 GeV using the ultrarelativistic quantum molecular dynamics model

Khaled Abdel-Waged*

Umm Al-Qura University, Faculty of Applied Science, Physics Department, Makkah Unit 126, P.O. Box 7047, Saudi Arabia

The ultrarelativistic quantum molecular dynamics (UrQMD) model is incorporated with a statistical decay model aiming to describe the neutron double global-differential cross sections of $p+$Al, Fe, and Zr at 1.2 GeV. Good agreement is generally obtained with the default UrQMD parameters. In particular, the UrQMD calculation with a momentum dependent Pauli potential improves the intensity of the quasielastic peak in neutron double-differential cross sections. The lower and higher energy parts of the neutron spectra at backward angles are found to be sensitive to meson-meson and meson-baryon interactions. The influence of sequential evaporation and simultaneous multifragmentation disintegration mechanisms on the neutron spectra is also investigated. It is shown that the statistical multifragmentation model is more suited for the description of the lower part of the neutron energy spectra.

I. INTRODUCTION

In recent years, spallation reactions have come to be more and more important for various reasons related with not only the basic but also the applied research field. Applications of these reactions include generation of high intensity beams of neutrons [1], transmutation of nuclear wastes [2–4], and/or developing a new type of nuclear reactor [5,6].

A spallation reaction is generally described as a two-step process. In the first step, the nonequilibrium process, the primary nucleon-nucleus interactions is treated as a succession of nucleonic and mesonic interactions with the nucleons of the target nucleus, as described by microscopic transport models [7–12]. In the second step, the equilibration process, the resulting excited nucleus is allowed to cool by particle evaporation, as described by statistical models [13–15].

Over the last years, various versions of hybrid (microscopic plus statistical) models have been developed to describe spallation data at intermediate energies (1–3 GeV) [16–18]. Their results, however, cannot predict the whole spectra of spallation produced neutrons. In particular, a systematic deviation from the data is found in the high energy part of the neutron spectra at the most forward angles. Possible causes are the absence of momentum dependent interactions and/or the differential cross section of in-medium nucleon-nucleon (NN) elastic scattering. Such effects, although pointed out in Refs. [16–18], have not practically been tested. Therefore, in order to investigate these effects, a two-step model is employed, namely, we incorporate the ultrarelativistic quantum molecular dynamics (UrQMD) model [12] for the nonequilibrium process with a statistical decay model [14]. The UrQMD model offers several advantages in comparison with other currently used nonequilibrium models: (i) it includes all baryonic resonances up to an invariant mass of 2 GeV as well as mesonic resonances up to 1.9 GeV as tabulated by the Particle Data Group [19]; (ii) it incorporates mean field dynamics (with and/or without momentum dependent Pauli potential); (iii) it implements the in-medium differential cross section of NN-elastic scattering [20].

Since spallation reactions are quite effective in bringing nuclei to a broad distribution of excitation energies, we will also investigate to which extent the well known sequential evaporation (SE) [13] and simultaneous multifragmentation (SM) [14] (statistical) models are suitable for the description of the lower part of the neutron energy spectra.

The paper is organized as follows. Section II defines the basic ingredients of the UrQMD plus SM model and discusses how these two are combined. In Sec. III, we apply this model systematically to the recent measured [21] double-differential cross sections of the neutron yield as a function of the kinetic energy (E_n) at fixed angles from 0° to 160° for $p+$Al, Fe, and Zr interactions at 1.2 GeV. We summarize and conclude this work in Sec. IV.

II. DESCRIPTION OF THE COMBINED MODEL

Here we describe the outline of the UrQMD plus SM model. The detail of UrQMD is described in Ref. [12]. The main components of UrQMD are as follows.

Nuclear collisions are assumed to be described by the sum of independent binary hadron-hadron (hh) collisions. Each hh collision is assumed to take place at the distance of closest approach, that is, two particles collide if their distance d_{trans} fulfills the relation:

$$d_{trans} \leqslant \sqrt{\frac{\sigma_{tot}}{\pi}}, \quad \sigma_{tot} = \sigma(\sqrt{s}, \text{type}). \quad (1)$$

The total cross section σ_{tot} depends on the center-of-mass energy ($\sqrt{s}$) and on the species and quantum number of the incoming particles. d_{trans} is defined as the covariant relative distance between the two particles:

─────────
*Permanent address: Physics Department, Faculty of Science, Benha University, Benha, Egypt. Email address: khelwagd@yahoo.com

$$d_{trans} = \sqrt{(\vec{r}_1 - \vec{r}_2)^2 - \frac{[(\vec{r}_1 - \vec{r}_2)\cdot(\vec{p}_1 - \vec{p}_2)]^2}{(\vec{p}_1 - \vec{p}_2)^2}}$$

with $\vec{r}_i$ being the locations and $\vec{p}_i$ the momenta in the local rest frame of the colliding particles.

The inelastic hh collisions produce resonances at low and intermediate energies, while at high energies ($\sqrt{s}=5$ GeV for baryon-baryon and 3 GeV for meson-baryon and meson-meson reactions) color strings are formed and they decay into hadrons according to the Lund string model [23]. There are 55 baryon and 32 meson states as discrete degrees of freedom in the model as well as their antiparticles and explicit isospin projected states with masses up to 2.25 GeV/c^2. All of these hadronic states can propagate and reinteract in phase space.

An analytical expression for the differential cross section of in-medium NN elastic scattering derived from the collision term of the relativistic Boltzmann-Uehling-Uhlenbeck (RBUU) equation [22] is used to determine the scattering angles between the outgoing particles in elementary hh collisions.

The Pauli principle is applied to hadronic collisions by blocking the final state if the outgoing phase space is occupied.

On the basis of quantum molecular dynamics, potential interactions are enforced for the scattered nucleons. The single particle wave function of each nucleon is represented by a Gaussian wave packet, having the phase-space centroid parameters of $\vec{R}_i$ and $\vec{P}_i$ for the ith nucleon. The total wave function is assumed to be a product wave function of nucleon Gaussian wave packet. The equation of motion for their centeroids ($\vec{R}_i$ and $\vec{P}_i$) is given by

$$\frac{dR_j}{dt} = \frac{\partial H}{\partial P_j}, \quad \frac{dP_j}{dt} = -\frac{\partial H}{\partial R_j}. \tag{2}$$

The Hamiltonian H consists of the kinetic energy and the effective interaction energy,

$$H = T + V,$$

$$T = \sum_j [(p_j^2 + m_j^2)^{1/2} - m_j],$$

$$V = V_{Skyrme} + V_{Yukawa} + V_{Coulomb} + V_{Pauli}. \tag{3}$$

In this interaction energy, the following terms are included: Skyrme type density dependent interaction (V_{Skyrme}), Yukawa potential (V_{Yukawa}), Coulomb potential between protons ($V_{Coulomb}$), and the Pauli potential (V_{Pauli}). The form of each term is given by

$$V_{Skyrme} = \frac{t_1}{2\rho_0} \sum_{i=1}^{A} \sum_{\substack{k=1 \\ k\neq i}}^{A} \tilde{\rho}_{ik} + \frac{t_\gamma}{(\gamma+1)\rho_0^\gamma} \sum_{i=1}^{A} \left(\sum_{\substack{k=1 \\ k\neq i}}^{A} \tilde{\rho}_{ik} \right)^\gamma,$$

TABLE I. Parameters of the UrQMD model for different interactions.

Parameter	Without Pauli potential	With Pauli potential
α (fm^{-2})	0.25	0.1152
t_1 (MeV fm^3)	-163.0	-84.5
t_γ (MeV fm^6)	125.95	188.2
γ	1.676	1.46
V_0^{Yuk} (MeV fm)	-0.498	-85.1
γ_Y (fm)	1.4	1.0
V_0^{Paul} (MeV)		99.5
q_0 (fm)		3
p_0 (MeV/c)		120

$$V_{Yukawa} = \frac{V^{Yuk}}{2} \sum_{i=1}^{A} \sum_{\substack{k=1 \\ k\neq i}}^{A} \frac{1}{2\vec{r}_{ik}} \exp\left(\frac{1}{4\alpha\gamma_Y^2} \right)$$

$$\times \left\{ e^{-\vec{r}_{ik}/\gamma_Y} \left[1 - \text{erf}\left(\frac{1}{2\gamma_Y\sqrt{\alpha}} - \sqrt{\alpha}\vec{r}_{ik} \right) \right] \right.$$

$$\left. - e^{\vec{r}_{ik}/\gamma_Y} \left[1 - \text{erf}\left(\frac{1}{2\gamma_Y\sqrt{\alpha}} + \sqrt{\alpha}\vec{r}_{ik} \right) \right] \right\},$$

$$V_{Coulomb} = \frac{1}{2} e^2 \sum_{i=1}^{A} \sum_{\substack{j=1 \\ j\neq i}}^{A} \frac{1}{r_{ij}} \text{erf}(\sqrt{\alpha}r_{ij}),$$

$$V_{Pauli} = \frac{1}{2} V_0^P \left(\frac{\hbar}{p_0 q_0} \right)^3 \left(1 + \frac{1}{2\alpha q_0^2} \right)^{-3/2}$$

$$\times \sum_{i=1}^{A} \sum_{\substack{k=1 \\ k\neq i}}^{A} \exp\left(\frac{-\alpha r_{ik}^2}{2\alpha q_0^2 + 1} - \frac{p_{ik}^2}{2p_0^2} \right) \delta_{\tau_i\tau_k} \delta_{\sigma_i\sigma_k}, \tag{4}$$

where $\vec{r}_{ik} = \vec{R}_i - \vec{R}_k$, $\vec{p}_{ik} = \vec{P}_i - \vec{P}_k$, τ_i, and σ_i denote the spin-isospin index of nucleon (i), and the "interaction density" $\tilde{\rho}_{ik} = (\alpha/\pi)^{3/2} e^{-\alpha(\vec{R}_i - \vec{R}_k)^2}$.

The summation runs over all projectile and target nucleons, $\rho_0 = 0.168$ fm^{-3} is the normal nuclear density, and erf denotes the error function. The values of the potential parameters appearing in Eq. (4) are listed in Table I.

The ground state configuration is obtained by the following random packing procedure. The centeroids of the Gaussians $\vec{R}_i$ are randomly distributed within a sphere with radius

$$R = 1.124[\tfrac{1}{2}[A + (A^{1/3} - 1)^3]]^{1/3}, \tag{5}$$

where A is the mass number of the nucleus. In choosing $\vec{R}_i$ a minimum distance of 1.6 fm between the centers of the Gaussians is imposed. The initial momenta of the nucleons are randomly chosen between 0 and the local Thomas-Fermi momentum: $p_F^{max} = \hbar c(3\pi^2\rho)^{1/3}$, with ρ being the corresponding local-proton or neutron density. The phase space density at the location of each nucleon is evaluated: if the
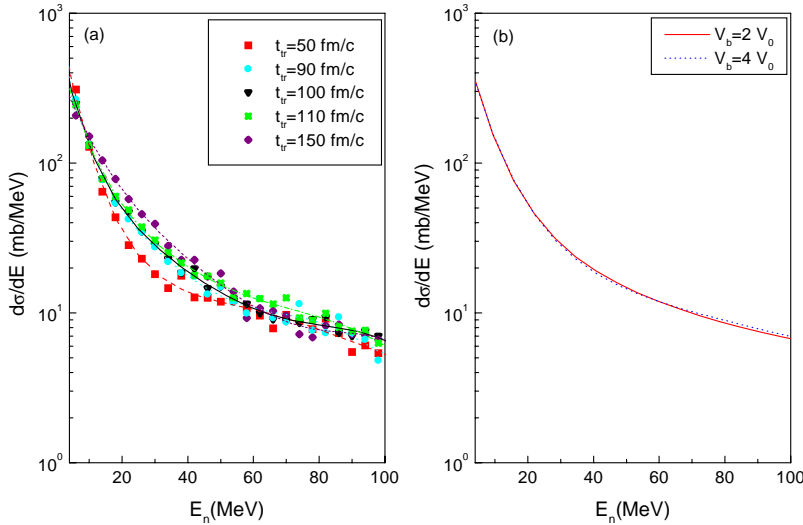
FIG. 1. (Color online) The total neutron energy spectra for $p(1.2 \text{ GeV}) + \text{Zr}$ interactions calculated by UrQMD (without Pauli potential) plus SM model with different transition times t_{tr} (a) and freeze-out volumes V_b (b). The lines are the best fit to the results.

phase space density is too high, then the location of that nucleon is rejected and a new location is randomly chosen. This procedure reduces fluctuations in the mean density of the nucleus.

The UrQMD calculation is carried out up to a time scale referred to as the transition time t_{tr}. The position of each nucleon is then used to calculate the distribution of mass and charge numbers (referred to as ''prefragments''). In determining the mass and charge numbers of the prefragments, the minimum spanning tree method [24] is employed, a prefragment is formed if the centroid distances are lower than R_{clus}. The most accepted range of R_{clus} is between 2 and 5 fm [24]. In this paper, R_{clus} is fixed at 3 fm. There are also new clusterization algorithms reported in the literature [25]. But the different clusterization algorithms give the same distribution at very late time, when the clusters are well separated from each other.

The total energy of each prefragment is determined in its rest frame by the Lorentz transformation. The excitation energy (ϵ^*) of the hot prefragments is calculated as the difference between the binding energy of the hot prefragments and the binding energies of these prefragments in their ground state.

The ensemble of prefragments is characterized by excitation energy ϵ^*, nucleon A_0, and proton Z_0, numbers. The decay of the residual nuclei is described by the SM model [14]. The SM model assumes that a hot nucleus expands to a freeze-out volume where it splits into primary hot prefragments and nucleons in thermal equilibrium. Obviously, the volume is a free parameter of the model. The volume is generally [14] defined as $V_b = (1+k)V_0$, $k \sim 2-3$, and V_0 is the volume of A_0 nucleon system in the ground state. The breakup channels are constrained by the total mass, charge, and energy of the system. All prefragments (and nucleons) are considered as Boltzmann particles while Fermi gas approximation is used for their internal excitation. The probabilities of different breakup channels are calculated according to their statistical weights. After primary breakup excited prefragments propagate independently under mutual Coulomb field and undergo secondary decay. This secondary dis-

integration of large fragments ($A > 16$) is described by an evaporational model [13], for smaller fragments the Fermi breakup model [28] is used.

Let us now investigate whether the results of the final observables would depend on the choice of V_b and t_{tr}, which determine, respectively, the configuration of the system at the end of the first stage and the time chosen to end the molecular dynamics calculation and start the afterburner mechanism. This is shown in Fig. 1, where we plot results of the total neutron spectra for $p(1.2 \text{ GeV}) + \text{Zr}$ interactions calculated by the UrQMD (without Pauli potential) plus SM model as a function of t_{tr} [Fig. 1(a)] and V_b [Fig. 1(b)].

Figure 1(a) shows that, although the total neutron spectra calculated with $t_{tr} \gtrsim 90 \text{ fm}/c$ resemble each other, they deviate definitely from $t_{tr} = 50 \text{ fm}/c$. This indicates that the UrQMD prefragments before 90 fm/c are not in thermal equilibrium and that within a time interval from 90 fm/c to 150 fm/c the decay processes of the excited prefragments described by the UrQMD plus SM model are nearly equivalent. Although we should keep in mind that the calculated neutron spectra are not identical at $t_{tr} \sim 100 \text{ fm}/c$ and $t_{tr} = 150 \text{ fm}/c$, we can conclude that the final results are not sensitive to t_{tr} as long as it is chosen after the time when thermal equilibrium is achieved and before the time the temperature of the prefragments becomes low and classical statistics [29] breaks down seriously. We found, as in Refs. [16–18], that $t_{tr} = 100 \text{ fm}/c$ is enough to get stable results and we use this value for all systems in the present study.

In Fig. 1(b) we check the dependence on the freeze-out volume V_b, when the UrQMD calculation is stopped at 100 fm/c and switched to SM model. As one can see, the total neutron spectrum shape is not sensitive to the choice of V_b. In model calculations presented below we take, as in Refs. [14,26,27]), $V_b = 3 V_0$.

In the numerical calculations, the URQMD (version 1.2) is run in two modes, the mean field mode without Pauli potential (UrQMD/$M1$) and the one which incorporates the whole mean field (with Pauli potential) (UrQMD/$M2$). In both modes, the prefragments together with their excitation energies are identified at 100 fm/c.
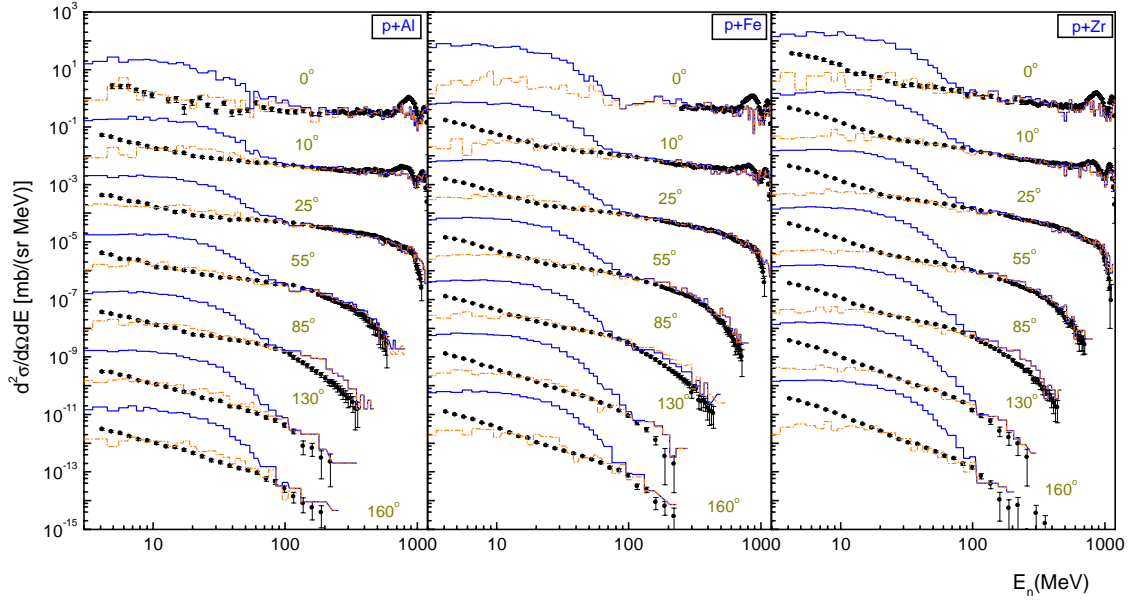
FIG. 2. (Color online) The experimental (error bars) neutron double-differential cross sections as a function of neutron kinetic energy (E_n) for p + Al (left), Fe (middle), and Zr (right) interactions at 1.2 GeV in the angular interval from 0° to 160°, as compared to UrQMD/$M1$ calculations. Solid histograms denote calculations without clusterization. Dot dashed histograms denote calculations with clusterization. For clarity, only the histograms and the data for the smallest angle are given in absolute value. The other ones have been multiplied by 10^{-2}, 10^{-4}, ..., for other angles in increasing order.

III. RESULTS AND DISCUSSION

In this section, we display the predictions of the UrQMD model along with the recent measurements [21] of double-differential neutron production cross sections as a function of E_n at various angular intervals from 0° to 160° for p + Al, Fe, and Zr at 1.2 GeV.

The measured energy spectra (see Figs. 2, 4, and 6) show that at 0° two prominent peaks appear. These two peaks are less pronounced at 10° and are insignificant at 25° and larger. In addition to these two peaks, it seems that two components exist for all of the spectra: one is a shoulder below $E_n \sim 10$ MeV, the other is a wide peak extending up to a few hundred MeV. The energy spectra below $E_n \sim 10$ MeV show an almost identical shape for all of the spectra. These low energy neutrons could be attributed to evaporation from target residues through the equilibration process. The other component becomes less pronounced with increasing angles. This component may reflect the nonequilibrium process. We note that the three components exist for all spallation reactions induced by an intermediate energy (around 1 GeV) proton on various targets [17,21]. Below we are going to investigate these three components by employing the UrQMD model with a statistical decay model. We performed 10 000 simulations at various impact parameters from 0 to R + 0.5 fm, where R is the target radius given by Eq. (5). It should be mentioned that the transport in the target (3-cm thick for Al, Fe, and Zr) is not evaluated here. This amounts to roughly a constant shift of the curves in the semi-logarithmic plots shown in Fig. 2 and similar ones toward low energies. However, due to the smooth variation of the curves and the scales, this correction would not be visible.

In Fig. 2 we compare the UrQMD/$M1$ calculations with-

out (solid histograms) and with (dot-dashed histograms) clusterization along with the whole experimental neutron spectra. The former calculations show a broad maximum at $E_n \sim 3$–10 MeV and then a fast decrease with increasing E_n up to $E_n \sim 100$ MeV, in all angular intervals for all studied interactions. As one can see, this maximum is counted in the UrQMD/$M1$ calculations (with clusterization) as a collection of individual nucleons, which is disregarded in the standard UrQMD approach. The importance of clusterization increases when both the mass of the target system and the observed angle increase. The figure also shows that the UrQMD/$M1$ calculations (dot-dashed histograms) well fits the experimental spectra above $E_n \sim 6$, 8, and 13 MeV for p + Al, Fe, and Zr, respectively, which directly reflects the multiple scattering picture and/or the nonequilibrium process included in the UrQMD model.

The lower part of the neutron energy spectrum (below $E_n = 6$, 8, and 13 MeV) can be treated by coupling the UrQMD/$M1$ with a statistical decay model. Among the statistical models, the SE and SM models are frequently applied. The former is used for an analysis of (p, xn) reactions (Refs. [16–18]), while the latter for the description of experimental data on fragment production (Refs. [26,27]). The sequential emission of particles by evaporation from the compound nucleus or its fission are the basic deexcitation mechanisms of the SE model. Within the SM model, the decay process is considered as a simultaneous break-up of the system into nucleons and fragments which later undergo secondary breakup (for $A < 16$) or evaporation (for $A > 16$). It would be interesting to study the effect of the different decay models on the neutron spectra in order to test their validity and understand their difference, using always the
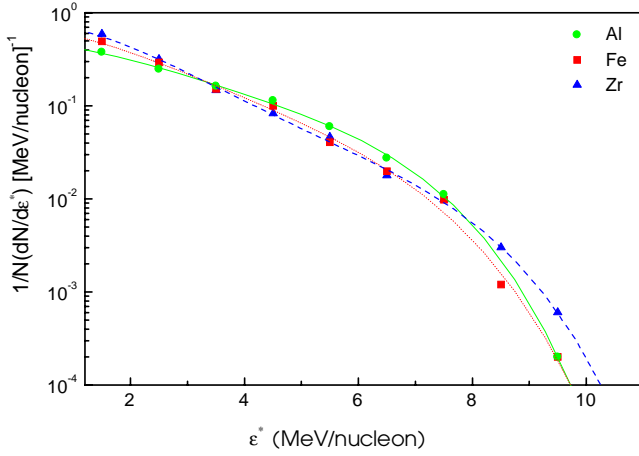
FIG. 3. (Color online) Calculated excitation energy distributions of prefragments after the UrQMD/$M1$ initiated by a proton on Al (solid circles), Fe (solid squares), and Zr (solid triangles) at 1.2 GeV. The lines are the best fit to the results.

same UrQMD(/$M1$) model. In order to compare these two decay models precisely, the evaporational process of the SM model was simulated by the same algorithm used in the SE model. In the following, the UrQMD/$M1$ calculations after SE and SM models are denoted as "UrQMD/$M1+SE$" and "UrQMD$+SM$," respectively.

Before going any further, it is of interest to look at the excitation energy distribution of prefragments obtained with UrQMD/$M1$ calculations. This is shown in Fig. 3 for all studied interactions. As seen from the figure, the excitation energy spectrum of the prefragments extends from the minimal values up to $\epsilon^* \sim 10$ MeV/nucleon. Therefore, the products of both decay mechanisms, the evaporation and fragmentation, should be present in proton-nucleus reactions. A

similar conclusion has been obtained in Ref. [14], for p + Ag interactions.

In Fig. 4 we compare both the UrQMD/$M1+SM$ (thin solid histograms) and UrQMD/$M1+SE$ (dashed histograms) calculations with the experimental neutron energy spectra for the studied interactions. In the case of $p+$ Al interactions, both calculations can nicely describe the slow evaporated neutron spectra. However, lesser emission of slow neutrons is followed in UrQMD/$M1+SM$ compared to UrQMD/$M1+SE$. As for $p+$ Fe ($p+$ Zr) interactions lesser emission of slow neutrons is observed in UrQMD/$M1$ $+SM$ compared to UrQMD/$M1+SE$ at $\theta \leq 25°$, especially at $E_n \geq 9$ MeV. Starting at $\theta > 25°$, UrQMD/$M1+SM$ generates a slight (large) excess of slow neutrons compared to UrQMD$+SE$ for $p+$ Fe ($p+$ Zr) interactions.

These results can tentatively be explained by investigating Fig. 5. At small scattering angles ($\theta \leq 25°$) (peripheral interactions) large Fe and Zr prefragments are mostly produced with $\langle \epsilon^* \rangle < 3$ MeV/nucleon. At such excitation energies the successive emission of particles by evaporation from the compound nucleus or its fission are the basic deexcitation mechanisms. In this case the UrQMD/$M1+SE$ should yield more slow neutrons than UrQMD/$M1+SM$, as shown in Fig. 4. At large scattering angles ($\theta > 25°$) (semicentral and central interactions) the Fe and Zr nuclei may break into medium and large prefragments ($A/3 < \langle A_0 \rangle < A$) which acquire, according to Fig. 5, an excitation energy ranging for different $\langle A_0 \rangle$ from 3 to 6 MeV/nucleon. In this excitation energy range, UrQMD/$M1+SM$ becomes more effective in producing more slow neutrons compared to UrQMD/$M1$ $+SE$, since the SM model breaks the Fe and Zr prefragments into many hot fragments with $A \geq 16$ which later enhance the number of slow neutrons through evaporation. On the other hand, for $p+$ Al interactions the main role is played
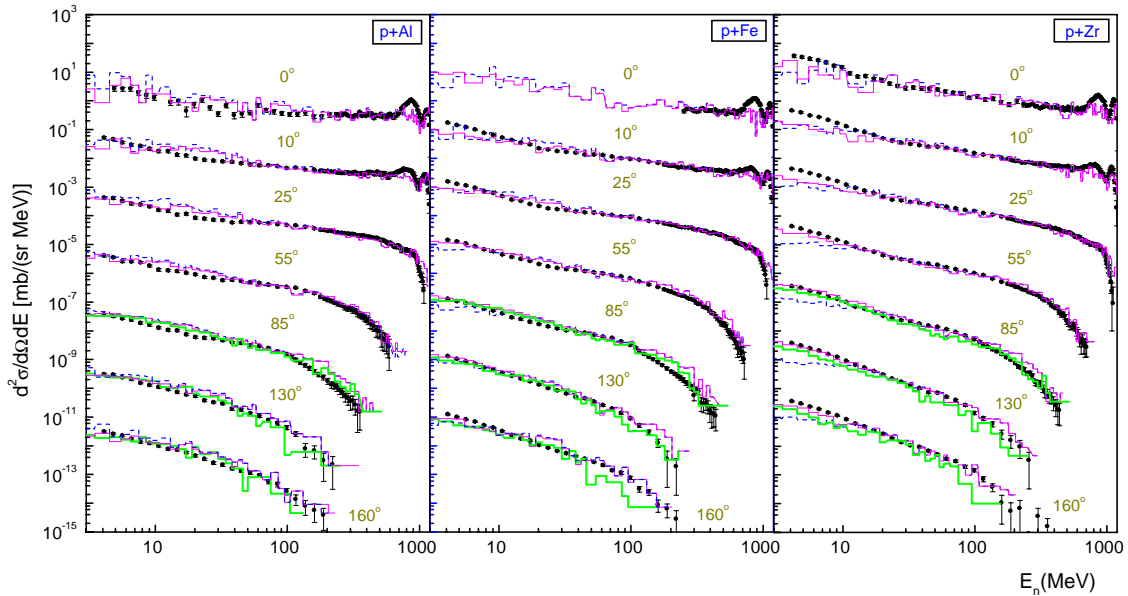

FIG. 4. (Color online) Same as Fig. 2, but here the thin solid and small dashed histograms denote the UrQMD/$M1+SM$ and UrQMD/$M1+SE$ calculations, respectively. The thick solid histograms denote the UrQMD/$M1+SM$ calculations without meson-meson and meson-baryon interactions.
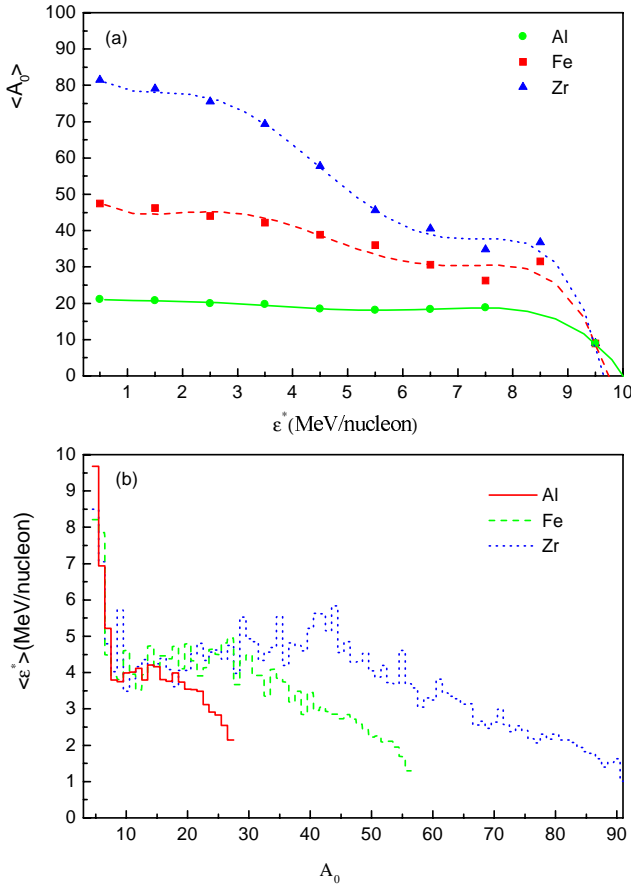
FIG. 5. (Color online) The correlations between the excitation energy per nucleon ϵ^* and the mass number of prefragments A_0 for the reactions under study. (a) The dependence of $\langle A_0 \rangle$ on ϵ^*. (b) The dependence of $\langle \epsilon^* \rangle$ on A_0. The lines (a) and histograms (b) denote the UrQMD/$M1$ calculations.

by the compound nucleus mechanism (sequential evaporation) at all angular intervals, as most of the $A_0 \geq 16$ prefragments are produced with a narrow range of $\langle \epsilon^* \rangle$ of about 3 MeV/nucleon [see Fig. 5(b)].

One may also notice that the evaporation part of the spectra slightly deteriorates as the angle is decreasing for $p + $ Fe and Zr interactions: the predicted slope has a tendency to become too small compared to the data. We found from detailed comparison of the calculations that the underestimation of slow evaporated neutrons in the above decay models is due to either a too large predicted excitation energy in the UrQMD/$M1$ model or a too small level density parameter used in the SE model. This tendency of underestimation was also reported in Ref. [17] using the INCL4 model.

In Fig. 4, we additionally study the influence of secondary interactions on the neutron spectra. Two different scenarios are explored: UrQMD/$M1 +$ SM calculations with the full collision term (thin lines) are contrasted by UrQMD/$M1$ $+$ SM simulations with deactivated meson-meson and meson-baryon interactions (thick lines). Note that in the latter not only multiple baryon-baryon interactions are allowed, but also baryon-antibaryon annihilations are still possible. Calculations with and without rescattering coincide in the

forward angles ($\theta < 85°$). However, in the backward angles ($\theta \geq 85°$) the calculation without rescattering (thick lines) gives lower values in both the low and high energy parts of the neutron spectra for all studied interactions. At very backward angles ($\theta \geq 130°$), it has been reported that the Cugnon intranuclear cascade model (INCL) fails to reproduce the neutron spectra for the studied interactions [21]. The underestimation of the backward angles in INCL model is thus due to the insufficient treatment of meson-meson(baryon) interactions mixed with soft interactions [Eqs. (4)], which is naturally included in the UrQMD/$M1$ formalism.

Finally, let us investigate the quasielastic and quasiinelastic processes seen at the high energy part of the most forward angles for the interactions under study. In the former process, the incident proton hits a neutron elastically, which leaves the nucleus without any further interaction [a single (p, n) elastic scattering]. In the latter process, the incident proton is excited to a Δ resonance, whereas the neutron is still emitted without further interaction [a single (p, n) inelastic scattering]. This is illustrated by Fig. 6, which shows a closeup of this region. Here the UrQMD/$M1$ is contrasted by the UrQMD/$M2$ (with the full potential). As one can see, the intensity of the quasielastic peak, i.e., the bump in the neutron energy spectrum close to the beam energy, is well reproduced at $0°$ and $10°$ by both calculations. One may, however, notice that the width of the intensity becomes wider and closer to the data in the case of UrQMD/$M2$ compared to UrQMD/$M1$. This may indicate the importance of the momentum dependent Pauli potential, by which the nucleon could be affected coherently by the surrounding nucleons when its momentum is drastically changed by the hard nucleon-nucleon scattering. As for the quasi-inelastic peak, i.e., the peak located at the beam energy minus ~ 300 MeV, the agreement is less satisfactory at $0°$, for both calculations. The lack of yield of high energy neutrons at the most forward angles seems to come from a too strong reinteraction in the UrQMD $[/M1(/M2)]$ model. There is, however, a tendency for the predictions to be better as both the target size and the angle increase. This may tentatively be ascribed to better and better conditions for the validity of the UrQMD $[/M1(/M2)]$ model. It can also be seen that there is no clear difference between the results of different UrQMD calculations in the quasi-inelastic region. This may be ascribed to the superposition of the single (p,n) inelastic scattering contribution with a background of multiple scattering contribution.

It should be noted that the quality of the results presented here see Refs. [17,21] for a comparison), especially for the quasielastic and inelastic peaks, is partly due to the UrQMD implementation of the differential cross section of inmedium NN elastic scattering.

IV. SUMMARY AND CONCLUSIONS

The UrQMD model is supplemented with a clusterization procedure followed by a statistical decay model for the description of spallation reactions. Different UrQMD model scenarios are explored and tested against the recently measured neutron double-differential cross sections in proton in-
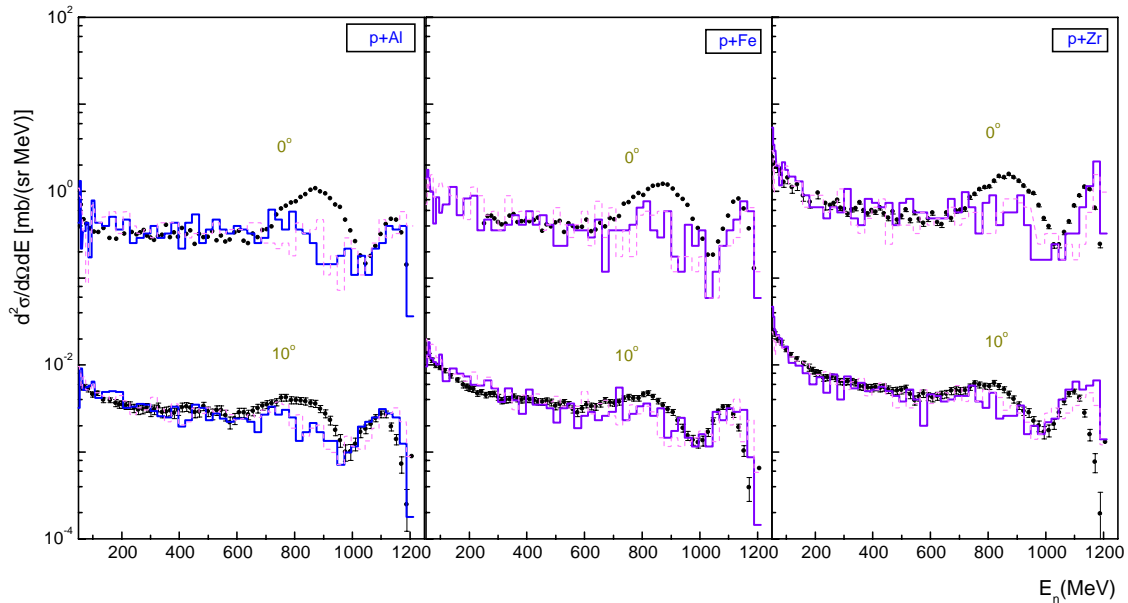
FIG. 6. (Color online) Same as Fig. 2 with a linear horizontal scale, but here the small dashed and solid histograms denote the UrQMD/$M1$ and UrQMD/$M2$ calculations, respectively.

duced reactions on Al, Fe, and Zr at 1.2 GeV. From such comparison, the following conclusions can be drawn.

Multiple scattering components [which correspond roughly to the interval 20 MeV, $E_{lab}/2$] are beautifully reproduced by UrQMD with mean field (without pauli potential) for the investigated reactions in all angular intervals.

The introduction of mean field with momentum dependent Pauli interactions improves the description of quasielastic peak.

Meson-meson and meson-baryon interactions affect both the lower and higher energy parts of the neutron spectra at backward angles ($\theta \geqslant 85$).

The statistical multifragmentation model (simultaneous breakup) is much better suited for the description of the slow evaporated neutron spectra for the reactions under study in all angular intervals.

The main ingredients of the UrQMD model, which produces the present results of the neutron spectra, are the parametrization of elastic and inelastic elementary cross sections, the implementation of the angular distribution of in-medium NN-elastic scattering process, and, finally, the many-

body dynamics. However, further possible improvements of the UrQMD model at intermediate energy are still needed. First, it would be important to take the in-medium Δ-relevant differential cross sections into account, i.e., in the study of quasiinelastic peak, rather than to replace all relevant two-body processes with the differential cross section of in-medium NN-elastic scattering. Second, it would be interesting to use a self-consistent minimization (e.g., via a Metropolis algorithm) of the energy of the initial nuclei using the full Hamiltonian (with Pauli potential), rather than using the normal packing procedure.

ACKNOWLEDGMENTS

[1] J.M. Carpenter, T.A. Gabriel, E.B. Iverson, and D.W. Jerng, Physica B **270**, 272 (1999).

[2] H. Arnould *et al.*, Phys. Lett. B **458**, 167 (1999).

[3] A. Abanades *et al.*, Nucl. Instrum. Methods Phys. Res. A **463**, 586 (2001).

[4] J.-S. Wan *et al.*, Nucl. Instrum. Methods Phys. Res. A **463**, 634 (2001).

[5] C.D. Bowman *et al.*, Nucl. Instrum. Methods Phys. Res. A **320**, 336 (1992).

[6] C. Rubbia *et al.*, preprint CERN/AT/95-44 (ET), 1995.

[7] G.F. Bertsch and S. Das Gupta, Phys. Rep. **160**, 189 (1988).

[8] J. Aichelin, Phys. Rep. **202**, 233 (1991).

[9] J. Cugnon, C. Volant, and S. Vuiller, Nucl. Phys. **A620**, 575 (1997).

[10] Khaled Abdel-Waged, Phys. Rev. C **59**, 2792 (1999); **67**, 024901 (2003).

[11] H. Sorge, Phys. Rev. C **52**, 3291 (1995).

[12] S.A. Bass *et al.*, Prog. Part. Nucl. Phys. **41**, 225 (1998).

[13] V. Weisskopf, Phys. Rev. **52**, 295 (1937); W.A. Friedman and W.G. Lynch, Phys. Rev. C **28**, 16 (1983).

[14] J.B. Bondorf *et al.*, Phys. Rep. **257**, 134 (1995).

[15] D.H.E. Gross, Rep. Prog. Phys. **53**, 3605 (1990).

[16] K. Niita *et al.*, Phys. Rev. C **52**, 2620 (1995); Y. Iwata, *et al.*, *ibid.* **64**, 054609 (2001).

[17] A. Boudard, J. Cugnon, S. Leray, and C. Volant, Phys. Rev. C **66**, 044615 (2002).

[18] Kh. Abdel-Waged, A. Abdel-hafiz, and V.V. Uzhinskii, J. Phys. G **26**, 1105 (2000).

[19] Particle Data Group, R.M. Barnett *et al.*, Phys. Rev. D **54**, 1 (1996).

[20] G. Mao, Z. Li, Y. Zhuo, and Y. Han, Phys. Rev. C **49**, 3137 (1994).

[21] S. Leray *et al.*, Phys. Rev. C **65**, 044621 (2002).

[22] G. Mao, Z. Li, and Y. Zhuo, Phys. Rev. C **53**, 2933 (1996).

[23] B. Andersson *et al.*, Nucl. Phys. **B281**, 289 (1987).

[24] Ch. Hartnack, Rajeev K. Puri, J. Aichelin, J. Konopka, S.A. Bass, H. Stocker, and W. Greiner, Eur. Phys. J. A **1**, 151 (1998).

[25] S. Leray, C. Ngo, P. Bouissou, B. Remoud, and F. Sebille, Nucl. Phys. **A531**, 171 (1991); P.B. Gossiaux, R.K. Puri, CH. Hartnack, and J. Aichelin, *ibid.* **A619**, 379 (1997).

[26] Khaled Abdel-Waged, Phys. Rev. C **63**, 024618 (2001); J. Phys. G **28**, 2951 (2002).

[27] EMU01 Collaboration, M.I. Adamovich *et al.*, Eur. Phys. J. A **1**, 77 (1998).

[28] E. Fermi, Prog. Theor. Phys. **5**, 570 (1950).

[29] A. Ohnishi and J. Randrup, Nucl. Phys. **A565**, 474 (1993).